

# **ScienceDirect**



IFAC PapersOnLine 54-20 (2021) 114-121

# Averaged Modeling of Pectoral Fin-Actuated Robotic Fish \*

Maria L. Castaño \* Xiaobo Tan \*\*

\* Department of Electrical and Computer Engineering, Michigan State University, East Lansing, MI 48824, USA (e-mail: castanom@msu.edu).

\*\* Department of Electrical and Computer Éngineering, Michigan State University, East Lansing, MI 48824, USA (e-mail: xbtan@eqr.msu.edu)

Abstract: Pectoral fins play an important role in the locomotion and maneuvering of robotic fish. Considering the cyclic nature of typical actuation modes, it is of interest to develop a dynamic average model that is amenable to controller design, where the control inputs are actuation pattern parameters. In this work, we propose a scaling-based approach to develop a nonlinear dynamic average model for a robotic fish propelled by a pair of rowing pectoral fins. In particular, the fin-generated hydrodynamic forces and moment, modeled using blade element theory, are scaled with functions of the fin-beat parameters, and classical averaging is then conducted over the corresponding modified dynamics. To determine proper scaling functions with minimal complexity, we propose a novel estimation scheme employing a nonlinear model predictive control formulation paired with a multivariate nonlinear regression scheme. Experimental and simulation results comparing the predictions from the dynamic and averaged models are presented to support the efficacy of the averaged modeling approach.

Copyright © 2021 The Authors. This is an open access article under the CC BY-NC-ND license (https://creativecommons.org/licenses/by-nc-nd/4.0/)

Keywords: Averaging, modeling, underwater vehicles, robotic fish, pectoral fins.

#### 1. INTRODUCTION

In the past few decades, robotic fish have received substantial attention due to their efficiency, maneuverability, and lifelike features. These characteristics make them an attractive choice for a myriad of aquatic applications such as environmental monitoring, search and rescue, and robotanimal interactions (Tan, 2011; Zhang et al., 2016; Marras and Porfiri, 2012). These robots have used various bioinspired propulsion methods, from oscillating caudal or pectoral fins to undulation of the entire body (Sfakiotakis et al., 1999). While caudal fins are typically used for efficient propulsion at higher speeds, pectoral fins are vital in assisting propulsion and achieving agile maneuvering at low swimming speeds (Behbahani, 2016).

Pectoral fin motions can generally be classified into three modes depending on the axis of rotation: rowing, feathering, and flapping, where the axes of rotation are vertical, transverse, and longitudinal, respectively. The rowing motion is classified as a "drag-based" swimming mechanism, and is particularly effective in achieving a number of inplane locomotion and maneuvering modes. Its fin-beat cycle comprises two sub-movements: the power stroke when the fin moves backward to produce thrust through induced drag on the pectoral fin surface, and the recovery stroke when the fin moves toward the front of the body, ideally with minimal loading, to get ready for the next fin-beat cycle.

There is extensive literature available on the prototype design and modeling of pectoral fin-actuated robotic fish (Sitorus et al., 2009; Palmisano et al., 2007; Ye et al., 2017; Kato, 1998: Lachat et al., 2006: Deng and Avadhanula, 2005: Mittal et al., 2006: Low and Willy, 2006: Behbahani, 2016: Lauder et al., 2006: Zhong et al., 2018: Duraisamv et al., 2019). Some of these works have focused on developing Computational Fluid Dynamics (CFD) models to carry out numerical analysis of the robot's hydrodynamic characteristics and the force generation of the fins. Despite being instrumental in studying pectoral fins' propulsive mechanism, CFD-based models are not suitable for control design. Some efforts have also gone into developing analytical models to study the propulsive mechanism and gait analysis. For example, Singh et al. (2019) and Bi et al. (2014) utilized blade element theory (BET) to evaluate the quasi-static hydrodynamic forces generated by undulating and rowing fins, respectively, and Liu et al. (2013) utilized Euler-Lagrange equation methods to develop a dynamic model for batoid swimming robots. Others have focused on developing modeling frameworks for analyzing the effects of different pectoral fin designs and materials on the robot's swimming performance and mechanical efficiency (Behbahani, 2016; Kodati et al., 2008; Sitorus et al., 2009; Kato and Inaba, 1998; Kato and Furushima, 1996), but these models are not amenable to controller design.

Given the rhythmic nature of the robotic fish's body and fin movements, averaging has proven to be a useful approach in obtaining control-affine models (Sanders et al., 2007; Bullo and Lewis, 2019), and studying the effect of

<sup>\*</sup> This research was supported in part by the National Science Foundation (DGE 1424871, IIS 1715714, IIS 1848945).

the input parameters on its dynamics and fins movement (Morgansen et al., 2002; Wang and Tan, 2015; Morgansen et al., 2007). Furthermore, in practical applications, it is more natural to control the parameters for periodic fin beats than directly controlling the fin position at every moment, which makes an averaged model best suited for trajectory planning and tracking control. To the best of our knowledge, the use of averaging has not been explored in developing control-affine models for pectoral fin-actuated robotic fish.

In this work, we present a nonlinear dynamic average model for robotic fish propelled by a pair of rigid pectoral fins undergoing rowing motion. In particular, we consider the robot undergoing planar motion, with its original dynamics incorporating pectoral fin-generated hydrodynamic forces evaluated via the blade element theory. Inspired by the work in Wang and Tan (2015), which deals with averaged dynamics for tail-actuated robotic fish, we seek scaling factors, as functions of fin-beat parameters, for the original hydrodynamic forces and moment, such that when classical averaging is applied to the resulting modified dynamics, the obtained average model produces locomotion behaviors close to those of the original dynamic model. One fundamental step in identifying the scaling functions is estimating the scaling values for a given finbeat pattern. Wang and Tan (2015) used a trial-and-error approach for the tail-actuated robotic fish, which is timeconsuming. We propose a systematic approach to finding optimal scaling values by formulating a novel nonlinear model-predictive control (NMPC) problem, which can be readily solved with NMPC packages. Once the scaling values are found for a set of fin-beat patterns, nonlinear regression is used to determine the scaling functions with minimal complexity. Simulation comparison between the averaged model and the original dynamic model, under finbeat patterns not used in identifying the scaling functions, supports the efficacy of the developed averaged model. Furthermore, we conduct experiments on a pectoral finactuated robotic fish and compare the experimental results with simulation predictions when considering the forward swimming motion, where both fins are actuated symmetrically.

The rest of the paper is organized as follows. We first review the dynamic model of the pectoral fin-actuated robotic fish in Section 2. In Section 3 we present the development of the proposed averaged model. In Section 4 we present the scheme to determine the averaged scaling functions, as well as the experimental and simulation validation of the resulting average model. Finally, we provide some concluding remarks in Section 5.

# 2. REVIEW OF THE DYNAMIC MODEL FOR PECTORAL FIN-ACTUATED ROBOTIC FISH

#### 2.1 Rigid Body Dynamics

We consider the robot to be a rigid body with rigid pectoral fins that are actuated at the base, and we assume that the robot operates in an inviscid, irrotational, and incompressible fluid within an infinite domain.

As illustrated in Fig. 1(a), we define  $[X,Y,Z]^T$  and  $[\hat{x},\hat{y},\hat{z}]^T$ as the inertial coordinate system and the body-fixed coor-

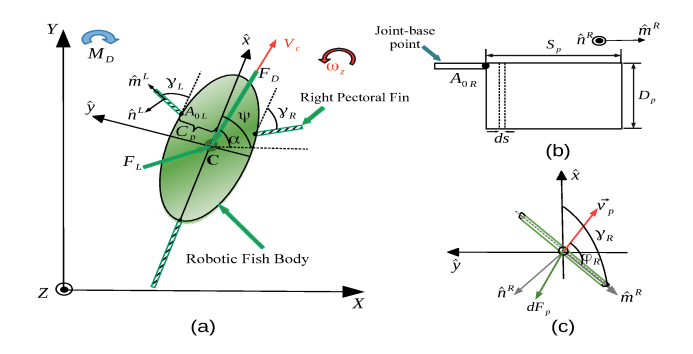


Fig. 1. (a) Top view of the pectoral fin-actuated robotic fish undergoing planar motion; (b) side view and blade element of the right pectoral fin with its parameters and variables; (c) top view of the pectoral fin with its associated forces and angles.

dinate system, respectively. We only consider the robot's planar motion, so the system only has three degrees of freedom, surge  $(v_{c_x})$ , sway  $(v_{c_y})$ , and yaw  $(\omega_z)$ . We let  $\alpha$ denote the angle of attack, formed by the direction of  $V_c$ , the linear velocity vector of the center of mass in the bodyfixed coordinate, with respect to the  $\hat{x}$ -axis, and is given by  $\alpha = \arctan(\frac{v_{c_y}}{v_{c_x}})$ . Let  $\psi$  denote the heading angle, formed by the  $\hat{x}$ -axis relative to the X-axis,  $C_p$  be the distance between the pectoral fin and the body's center of mass, while  $A_{0L}$  and  $A_{0R}$  denote the pivot points for the left and right fin, respectively. Finally,  $\gamma_L$  and  $\gamma_R$  represent the angles between the left pectoral fin and the body-fixed  $\hat{x}$ -axis and the right pectoral and the body-fixed  $\hat{x}$ -axis, respectively. Furthermore, we assume that we can neglect the inertial coupling between yaw, sway and surge motions (Aureli et al., 2009), and arrive at the following equations of planar motion

$$(m_b - m_{a_x})\dot{v}_{c_x} = (m_b - m_{a_y})v_{c_y}\omega_z - F_D\cos(\alpha) + F_L\sin(\alpha) + f_{h_x}$$
 (1)

$$(m_b - m_{a_y})\dot{v}_{c_y} = -(m_b - m_{a_x})v_{c_x}\omega_z - F_D\sin(\alpha) - F_L\sin(\alpha) + f_{h_y}$$
 (2)

$$(J_{bz} - J_{a_z})\dot{\omega}_z = (m_{a_y} - m_{a_x})v_{c_x}v_{c_y} + \tau_{h_z} + M_D$$
 (3)

where  $m_b$  is the mass of the body,  $J_{bz}$  is the inertia of the body about the z-axis,  $m_{a_x}$ , and  $m_{a_y}$  are the hydrodynamic derivatives that represent the added masses of the robotic fish along the  $\hat{x}$  and  $\hat{y}$  directions, respectively,  $J_{a_z}$ represents the added inertia effect of the body about the  $\hat{z}$  direction, and  $f_{h_x}$ ,  $f_{h_y}$ , and  $\tau_{h_z}$  are the hydrodynamic forces and moment transmitted to the robot's body by the right and left pectoral fins. Finally,  $F_D$ ,  $F_L$ , and  $M_D$  are the body drag, lift, and moment, respectively, and can be captured by (Wang et al., 2015; Morgansen et al., 2007)

$$F_D = \frac{1}{2}\rho |V_c|^2 S_A C_D \tag{4}$$

$$F_D = \frac{1}{2}\rho |\mathbf{V}_c|^2 S_A C_D$$

$$F_L = \frac{1}{2}\rho |\mathbf{V}_c|^2 S_A C_L \alpha$$

$$M_D = -C_M \omega_z^2 \operatorname{sgn}(\omega_z)$$
(5)

$$M_D = -C_M \omega_z^2 \operatorname{sgn}(\omega_z) \tag{6}$$

where  $\rho$  is the density of water,  $|V_c| = \sqrt{v_{c_x}^2 + v_{c_y}^2}$  is the linear velocity magnitude of the body in the body-fixed frame,  $S_A$  is the wetted surface area for the robot,  $C_D$  is the drag force coefficient,  $C_L$  is the lift force coefficient,  $C_M$ is the drag moment coefficient, and  $sgn(\cdot)$  is the signum function.

#### 2.2 Hydrodynamic Forces from Rowing Pectoral Fins

As shown in Fig. 1(b), we consider the pectoral fins to be rectangular with span length  $S_p$  and chord length  $D_p$ . We adopt the procedure presented by Behbahani and Tan (2016), and illustrate the force calculations using the right pectoral fin. However, it can be readily extended to the left pectoral fin.

We consider a coordinate system with unit vectors  $\hat{m}^R$  and  $\hat{n}^R$  that are attached to the pectoral fin (see Fig. 1) and are related to the robotic fish body-fixed coordinates as follows

$$\hat{m}^R = \cos \gamma_R \hat{x} - \sin \gamma_R \hat{y} \tag{7}$$

$$\hat{n}^R = -\sin\gamma_R \hat{x} - \cos\gamma_R \hat{y} \tag{8}$$

In the following calculations we assume an anchored robotic fish body, often adopted in literature as it simplifies calculation without incurring significant error (Behbahani, 2016; Valdivia y Alvarado and Youcef-Toumi, 2005). The velocity and acceleration at the point s along the fin are then given by

$$v_{p_R}(s,t) = s\dot{\gamma}_R \hat{n}^R \tag{9}$$

$$a_R(s,t) = s\ddot{\gamma}_R \hat{n}^R - s\dot{\gamma}_R^2 \hat{m}^R \tag{10}$$

where  $\dot{\gamma}_R$  and  $\ddot{\gamma}_R$  indicate the first and second time derivative of  $\gamma_R$ , respectively.

The hydrodynamic forces on the pectoral fin are composed of both span-wise and normal components. However, since the fins are considered to have pure rowing motion, the span-wise component that arises from friction is very small and can thus be neglected (Drucker et al., 2005). Using blade element theory, we can then calculate the differential normal force  $dF_{nR}(s,t)$  on each blade element ds on the pectoral fin at time t as

$$dF_{nR}(s,t) = -\frac{1}{2}C_n(\varphi_R(s,t))\rho D_p |v_{p_R}(s,t)|^2 ds \ \hat{n}^R \ (11)$$

where  $C_n(\varphi_R(s,t)) = \lambda \sin \varphi_R$  is the normal force coefficient, which depends on the angle of attack of each arbitrary blade,  $\varphi_R(s,t)$ , and  $\lambda$  is a parameter that can be evaluated empirically through experiments. The angle of attack of the right pectoral fin at each point,  $\varphi_R(s,t)$ , is defined as

$$\tan \varphi_R(s,t) = \frac{\langle v_{p_R}(s,t), \hat{n}^R \rangle}{\langle v_{p_R}(s,t), \hat{m}^R \rangle}$$
(12)

where  $\langle \cdot, \cdot \rangle$  denotes the inner product.

The total hydrodynamic force  $F_{n_R}$  and moment  $M_{n_R}$  (relative to its pivot point  $A_{0R}$ ) acting on the right pectoral fin are given by

$$F_{n_R} = \int_0^{S_p} \mathrm{d}F_{nR}(s,t) \tag{13}$$

$$M_{n_R} = \int_0^{S_p} s \hat{m}_R \times dF_{n_R}$$
 (14)

The total force acting on the right fin is determined by

$$\mathbf{F}_R = F_{n_R} \, \hat{n}^R - F_{A_0 R} = \left. m_p a_R(s, t) \right|_{s = \frac{S_P}{2}}$$
 (15)

where  $F_{A_0R}$  represents the force applied by the rigid pectoral fin on the servo joint, and  $m_p$  is the effective mass of the rigid fin (the fin mass  $m_{pf}$  and the added mass, where the added mass is calculated as shown in

Dong (1978)). Finally, the force and moment exerted on the robotic fish body by the right pectoral fin are given by

$$f_{h_{\pi}R} = \langle F_{A_0R}, \hat{x} \rangle \tag{16}$$

$$f_{h_y R} = \langle F_{A_0 R}, \hat{y} \rangle$$
 (17)

$$\tau_{h_R} = C_p \hat{y} \times F_{A_0 R} = -C_p f_{h_x R} \hat{k} \tag{18}$$

where  $<\cdot>$  denotes the inner product. By considering the kinematic equations of the robotic fish, the final dynamic model can be summarized as follows:

el can be summarized as follows:
$$\begin{bmatrix}
\dot{X} \\
\dot{Y} \\
\dot{\psi} \\
\dot{v}_{c_x} \\
\dot{v}_{c_y} \\
\dot{\omega}_z
\end{bmatrix} = \begin{bmatrix}
v_{c_x} \cos \psi - v_{c_y} \sin \psi \\
v_{c_x} \sin \psi + v_{c_y} \cos \psi \\
\omega_z \\
f_1(v_{c_x}, v_{c_y}, \omega_z) + \frac{f_{h_x R} + f_{h_x L}}{m_1} \\
f_2(v_{c_x}, v_{c_y}, \omega_z) + \frac{f_{h_y R} + f_{h_y L}}{m_2} \\
f_3(v_{c_x}, v_{c_y}, \omega_z) + \frac{\tau_{h_R} + \tau_{h_L}}{J_3}
\end{bmatrix}$$
(19)

where

$$\begin{cases} f_1(v_{c_x}, v_{c_y}, \omega_z) = \frac{m_2}{m_1} v_{c_y} \omega_z - \frac{c_1}{m_1} v_{c_x} \sqrt{v_{c_x}^2 + v_{c_y}^2} + \\ \frac{c_2}{m_1} v_{c_y} \sqrt{v_{c_x}^2 + V_{c_y}^2} \arctan(\frac{v_{c_y}}{v_{c_x}}) \\ f_2(v_{c_x}, v_{c_y}, \omega_z) = -\frac{m_1}{m_2} v_{c_x} \omega_z - \frac{c_1}{m_2} v_{c_y} \sqrt{v_{c_x}^2 + v_{c_y}^2} \\ -\frac{c_2}{m_2} v_{c_x} \sqrt{v_{c_x}^2 + v_{c_y}^2} \arctan(\frac{v_{c_y}}{v_{c_x}}) \\ f_3(v_{c_x}, v_{c_y}, \omega_z) = \frac{(m_1 - m_2)}{J_3} v_{c_x} v_{c_y} - c_4 \omega_z^2 \operatorname{sgn}(\omega_z) \end{cases}$$
(20)

with  $m_1 = m_b - m_{a_x}$ ,  $m_2 = m_b - m_{a_y}$ ,  $J_3 = J_{bz} - J_{a_z}$ ,  $c_1 = \frac{1}{2}\rho SC_D$ ,  $c_2 = \frac{1}{2}\rho SC_L$ ,  $c_4 = \frac{1}{(J_3)}C_M$ .

# 3. AVERAGING WITH SCALED FORCING

#### 3.1 Averaged Model

In order to generate a net thrust over each cycle, the pectoral fins need to be actuated differently in the power and recovery strokes. For example, to generate forward thrust the fin has to be actuated faster in the power stroke than in the recovery stroke. We specify the fin beat pattern as

$$\gamma(t) = \begin{cases} \gamma_0 - \gamma_A \cos\left[\pi \frac{(\zeta + 1)}{T_p} t\right], & 0 \le t \le \frac{T_p}{\zeta + 1} \\ \gamma_0 + \gamma_A \cos\left[\pi \left(\frac{\zeta + 1}{\zeta T_p}\right) (t - \frac{T_p}{\zeta + 1})\right], & \frac{T_p}{\zeta + 1} < t \le T_p \end{cases}$$
(21)

where  $\gamma_0$  is the fin-beat bias,  $\gamma_A$  is the fin-beat amplitude,  $T_P$  is the fin-beat period, and  $\zeta$  is a parameter defining the ratio of angular velocities of the fin during the power and recovery strokes, respectively.

Under this periodic fin movement, averaging can be a useful tool for gaining insight into the effect of the input parameters (such as the beat bias  $\gamma_0$ , amplitude  $\gamma_A$ , period  $T_p$ , and ratio  $\zeta$ ) on the dynamics and for designing controllers. First-order averaging (Bullo and Lewis, 2019) tends to generate prohibitively complex model for control (Wang and Tan, 2015). On the other hand, classical averaging (directly averaging the vector field over one period of the fin-beat) cannot be directly applied since the dynamics is not slow in typical scenarios as shown in Wang and Tan (2015). Therefore, we first scale the original forcing terms with functions that are potentially

dependent on the fin-beat parameters, and then apply classical averaging over the modified dynamics.

Specifically, let the original system (19) be modified as

$$\dot{v}_{c_x} = f_1(v_{c_x}, v_{c_y}, \omega_z) + K_{f_x R}(\gamma_{0R}, \gamma_{AR}, T_{pR}, \zeta_R) \cdot f_{h_x R}(t) + K_{f_x L}(\gamma_{0L}, \gamma_{AL}, T_{pL}, \zeta_L) \cdot f_{h_x L}(t)$$
(22)

$$\dot{v}_{c_y} = f_2(v_{c_x}, v_{c_y}, \omega_z) + K_{f_y R}(\gamma_{0R}, \gamma_{AR}, T_{pR}, \zeta_R) \cdot f_{h_y R}(t) + K_{f_y L}(\gamma_{0L}, \gamma_{AL}, T_{pL}, \zeta_L) \cdot f_{h_y L}(t)$$
(23)

$$\dot{\omega}_{z} = f_{3}(v_{c_{x}}, v_{c_{y}}, \omega_{z}) + K_{m_{R}}(\gamma_{0R}, \gamma_{AR}, T_{pR}, \zeta_{R}) \cdot \tau_{h_{R}}(t) + K_{m_{L}}(\gamma_{0L}, \gamma_{AL}, T_{pL}, \zeta_{L}) \cdot \tau_{h_{L}}(t)$$
(24)

where  $K_{f_xR}(\cdot), K_{f_yR}(\cdot), K_{m_R}(\cdot), K_{f_xL}(\cdot), K_{f_yL}(\cdot), K_{m_L}(\cdot)$  are scaling functions to be determined later (Section 4.3), and are  $\{\gamma_{0R}, \gamma_{AR}, T_{pR}, \zeta_R\}$  and  $\{\gamma_{0L}, \gamma_{AL}, T_{pL}, \zeta_L\}$  are the fin-beat parameters of the right fin and left fin, respectively. For brevity, the arguments of the functions  $f_1(\cdot), f_2(\cdot), f_3(\cdot)$  and the scaling functions are omitted in the remainder of the paper, and the calculations are illustrated using only the right fin since they can be extended for the left fin in a straightforward manner.

To avoid the integration of nested sin functions and facilitate the computation of the averaging, we first use the second-order Taylor series expansion to approximate the  $\cos(\gamma)$  and  $\sin(\gamma)$  terms that appear in the forcing terms in  $f_{h_x}$  and  $f_{h_y}$ . After conducting classical averaging, the following averaged system is obtained

$$\begin{cases} \dot{\bar{v}}_{c_{x}} = f_{1} + K_{f_{x}R} \cdot \bar{f}_{h_{x}R}(\gamma_{0R}, \gamma_{AR}, T_{pR}, \zeta_{R}) \\ + K_{f_{x}L} \cdot \bar{f}_{h_{x}L}(\gamma_{0L}, \gamma_{AL}, T_{pL}, \zeta_{L}) \\ \dot{\bar{v}}_{c_{y}} = f_{2} + K_{f_{y}R} \cdot \bar{f}_{h_{y}R}(\gamma_{0R}, \gamma_{AR}, T_{pR}, \zeta_{R}) \\ + K_{f_{y}L} \cdot \bar{f}_{h_{y}L}(\gamma_{0L}, \gamma_{AL}, T_{pL}, \zeta_{L}) \\ \dot{\bar{\omega}}_{z} = f_{3} + K_{m_{R}} \cdot \bar{\tau}_{h_{R}}(\gamma_{0R}, \gamma_{AR}, T_{pR}, \zeta_{R}) \\ + K_{m_{L}} \cdot \bar{\tau}_{h_{L}}(\gamma_{0L}, \gamma_{AL}, T_{pL}, \zeta_{L}) \end{cases}$$
(25)

where

$$\bar{f}_{h_x R} = \frac{D_p \lambda l_p^3 S_p^3 \pi^2 \rho \gamma_0 \gamma_A^2 (-4\gamma_0^2 - 3(-8 + \gamma_A^2))(-1 + \zeta^2)}{288 \zeta T_p^2}$$
 (26)

$$\bar{f}_{h_x R} = \frac{D_p \lambda l_p^3 S_p^3 \pi^2 \rho \gamma_0 \gamma_A^2 (-4\gamma_0^2 - 3(-8 + \gamma_A^2))(-1 + \zeta^2)}{288\zeta T_p^2}$$

$$\bar{f}_{h_y R} = \frac{-\gamma_A^2 l_p \pi^2}{96T_p^2 \zeta} \left( 4D_p \gamma_0^2 \lambda l_p^2 \rho (-1 + \zeta^2) + D_p (-8 + \gamma_A^2) \lambda l_p^2 \rho (-1 + \zeta^2) - 4\gamma_0^3 m_p (1 + \zeta)^2 - 3\gamma_0 \gamma_A^2 m_p (1 + \zeta)^2 \right)$$

$$(26)$$

$$\bar{\tau}_{h_R} = \frac{C_p D_p \lambda l_p^3 \pi^2 \rho \gamma_0 \gamma_A^2 (-4\gamma_0^2 - 3(-8 + \gamma_A^2))(-1 + \zeta^2)}{288\zeta T_p^2}$$
 (28)

Note that the model (25) can be expressed in a controlaffine form if one defines the control inputs as  $\alpha_1$  $K_{f_xR}\bar{f}_{h_xR}$ ,  $\alpha_2 = K_{f_xL}\bar{f}_{h_xL}$ ,  $\alpha_3 = K_{f_yR}\bar{f}_{h_yR}$  and  $\alpha_4 =$  $K_{f_{y}L}\bar{f}_{h_{y}L}$ . As an example, we refer the reader to Castaño and Tan (2019), where the authors show how one can express an averaged model for a trail-actuated robotic fish in a control-affine form and use it to design a modelpredictive controller.

## 4. SIMULATION AND EXPERIMENTAL RESULTS

In order to validate the presented averaged model, we must first identify the model hydrodynamic parameters

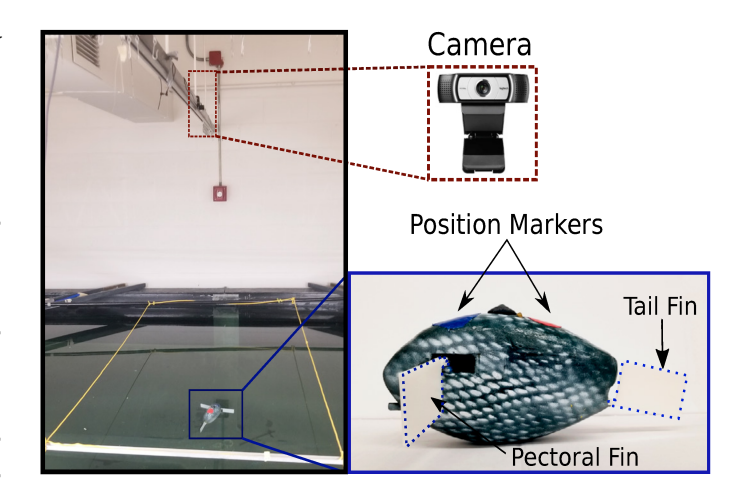


Fig. 2. The experimental setup. During experiments the pectoral-fin actuated robotic fish swims within the enclosed area (denoted by the yellow lines) in the tank, and the overhead Logitech camera captures a video of the robot swimming. An image processing algorithm detects the red and blue markers placed on top of the robot to localize it and determine its heading.

 $(C_D, C_L, \text{ and } C_M)$ , the fin parameter  $(\lambda)$ , and the scaling functions  $(K_{f_xR}, K_{f_yR}, K_{m_R}, K_{f_xL}, K_{f_yL}, K_{m_L})$ . In this section we present the experimental setup and discuss the experimental identification and validation of the hydrodynamic and fin model parameters and present an estimation scheme to obtain the scaling coefficients. Finally, we present simulation and experimental results to evaluate the effectiveness of the proposed averaged model.

#### 4.1 Experimental Setup

To validate the presented averaged model, we conduct experiments on the free-swimming robotic fish depicted in Fig. 2. The robot consists of a rigid-shell body, a tail and two rigid pectoral fins, which were all 3D-printed. Although the robot also has a servo-actuated caudal fin, the tail-actuation is not included in this work. The body and fins dimensions are shown in Tab. 1. Two Tenergy Li-Ion rechargeable batteries (7.4V, 3350mAh) are used to power the robot, and two Hitec digital micro waterproof servos (HS-5086WP) are used to actuate the pectoral fins according to (21). A Microchip Digital Signal Processor and Controller (DSPIC30F6014) is used to realize the control of the servos and a Xbee module is used for wireless communication with a computer.

The robotic fish is run in a 1.15 m by 2.30 m space enclosed within a tank equipped with an overhead Logitech C930E camera as seen in Fig. 2. To obtain the robotic fish's position and orientation in the tank, two markers were attached to the anterior and posterior of the robotic fish body. An overhead video of the robotic fish swimming in the tank is captured using the camera, and Visual C++ with the OpenCV library is used to implement an image processing algorithm. The algorithm detects the positions of the two markers and uses their average to obtain the center position of the robotic fish. In addition, the heading angle of the robot is estimated using the positions of the two markers, and a high gain observer is used to estimate

the linear and angular velocities of the robot based on the measured position and heading.

#### 4.2 Original Dynamics Parameter Identification

Before identifying the scaling functions and validating the averaged model, the hydrodynamic parameters present in the dynamic and averaged model must first be identified. These parameters are either measured directly or calculated based on measurements and are summarize in Tab. 1. As typically done in literature (Aureli et al., 2009; Behbahani and Tan, 2016), the body inertia about  $\hat{z}$ -axis is evaluated as  $J_{bz} = \frac{1}{5}m_b(a^2 + c^2)$ , where  $a = \frac{\text{Body lenght}}{2}$  and  $c = \frac{\text{Body width}}{2}$  are the semiaxis lengths. Furthermore, the added masses, added inertia, and wetted surface are calculated based on a prolate spheroid approximation of the robotic fish body (Aureli et al., 2009; Fossen, 1994).

The fin normal force coefficient  $\lambda$ , as well as the body drag and lift coefficients  $(C_D, C_L, \text{ and } C_M)$  are identified empirically from data collected using the robotic fish described above. In particular, we consider only turning motions which are achieved by activating only one fin at a time. To determine the body drag, lift and moment coefficients  $(C_D, C_L, \text{ and } C_M)$ , we let the robotic fish swim for some time (approximately 35 s) to reach the steady-state motion, and then stop actuating the pectoral fin such that the robot slowly halts to a stop. We use the captured video along with the image processing algorithm to determine the body-fixed velocities for different sets of fin amplitudes  $(\gamma_{AR})$ : 15°, 18°, 20°, 25°, 30°; biases  $(\gamma_{0R})$ : 80°, 90°, 100°, 110°; periods  $(T_{pR})$ : 0.5, 0.66, 1 s; and power/ recovery stroke ratios ( $\zeta$ ): 5, 6. Using the measured body-fixed velocities along with the dynamic equations (19) and a high gain observer to estimate the body-fixed acceleration, a parameter estimation algorithm is then employed to estimate the parameters. Furthermore, to estimate the fin parameter  $\lambda$ , we collect the robotic fish steady-state body-fixed velocities for another set of fin amplitudes  $(\gamma_{AR})$ : 8°, 10°, 13°, 15°, 18°; biases  $(\gamma_{0R})$ : 85°, 93°, 98°, 100°, 103°; periods  $(T_{pR})$ : 0.5, 0.66 s; and power/ recovery stroke ratios  $(\zeta)$ : 4, 5, and in a similar fashion estimate the parameter  $\lambda$ . The resulting coefficients are listed in Tab. 1. These parameters are then used in independent model validation for the dynamic and averaged models.

To validate the dynamic model, we conduct experiments based on different fin actuation parameters in both forward swimming and turning. In the forward swimming case both left and right fins are actuated in sync with the same finbeat patterns. We compare the steady state swimming speeds predicted by the model and those obtained from experiments in the forward swimming case, whilst in the turning cases we compare the turning radius and period. Each experiment is repeated four times to obtain the average and standard deviation. Tab. 2 and Tab. 3 lists the percent errors between the values obtained from experiments and those obtained from simulation using the parameters estimated earlier. The comparison indicates that the dynamic model has acceptable accuracy.

Table 1. IDENTIFIED MODEL PARAMETERS.

Robot Body		
Parameter	Value	unit
Body Length	0.198	m
Body Height	0.1	$\mathbf{m}$
Body Width $(C_P)$	0.03	m
Mass $(m_b)$	0.795	kg
Inertia $(J_{bz})$	$4.26 \times 10^{-4}$	${ m kg\cdot m^2}$
$-m_{ax}$	0.095	kg
$-m_{ay}$	0.1794	$_{ m kg}$
$-J_{az}$	$2.7\times10^{-5}$	${ m kg/m^2}$
Wet surface area $(S_A)$	0.325	$\mathrm{m}^2$
Drag coef. $(C_D)$	0.3870	-
Lift coef. $(C_L)$	0.0808	-
Moment coef. $(C_M)$	$8.5 \times 10^{-3}$	${\rm kg/m^2}$
Pectoral Fin		

Pectoral Fin		
Parameter	Value	$\operatorname{unit}$
Fin Length $(S_p)$	0.061	m
Fin Heigth $(D_p)$	0.041	$\mathbf{m}$
Fin Mass $(m_{pf})$	0.008	$_{ m kg}$
Effective mass $(m_p)$	0.008	kg
Water density $(\rho)$	1000	${ m kg/m^3}$
λ	4.1464	-

Table 2. MODEL VALIDATION RESULTS: RELA-TIVE MODEL PREDICTION ERROR FOR TURN-ING RADIUS AND TURNING PERIOD.

$(\gamma_{0L}, \gamma_{AL}, T_{pL}, \zeta_L)$	Turning Radius Error(%)	Turning Period Error(%)
(85°, 18°, 1 s, 4 )	10.96	5.96
$(85^{\circ}, 18^{\circ}, 1 \text{ s}, 3)$	4.66	17.92
$(80^{\circ}, 22^{\circ}, 1 \text{ s}, 4)$	12.67	4.91
$(80^{\circ}, 22^{\circ}, 1 \text{ s}, 3)$	16.15	2.12
$(85^{\circ}, 22^{\circ}, 1 \text{ s}, 4)$	2.60	1.39
$(85^{\circ}, 22^{\circ}, 1 \text{ s}, 3)$	13.61	4.82

Table 3. MODEL VALIDATION RESULTS: SURGE VELOCITIES PREDICTED BY THE ORIGINAL MODEL AND MEASURED FROM EXPERIMENTS, AND THEIR RELATIVE ERROR

	$(\gamma_{0L}, \gamma_{AL}, T_{pL}, \zeta_L)$	Surge Velocity(Experiments)	Surge Velocity(Model)	Error (%)
ĺ	(95°, 12°, 1 s, 4 )	0.0383	0.0397	3.60
ı	(95°, 12°, 0.66 s, 5)	0.0423	0.0449	5.77
ı	(100°, 12°, 0.8 s, 4)	0.0536	0.0494	8.52
ı	(100°, 12°, 0.8 s, 5)	0.0614	0.0558	9.96
ı	(100°, 12°, 0.66 s, 5)	0.0490	0.0447	9.74

#### 4.3 Identification of Scaling Functions

To identify the corresponding scaling functions for the averaged model, we conduct simulations using the original dynamic model (with the experimentally identified parameters) considering only one fin (the right fin) actuated with a given fin-beat pattern, and seek the corresponding values of the scaling functions (i.e.,  $K_{f_xR}$ ,  $K_{f_yR}$ ,  $K_{m_R}$ ) such that the resulting average model (25) produces the best match in the turning radius and turning period with those of the original dynamics (19).

Under a given fin actuation pattern, instead of conducting blanket-search of the scaling parameters as done in Wang and Tan (2015), we propose a novel formulation that treats the scaling values for the given actuation pattern as constant control inputs to the averaged model and solve for these values through nonlinear model predictive control (Allgöwer et al., 2004), such that the averaged system tracks the surge, sway, and angular velocities extracted from the simulated trajectory of the original dynamics (19) under the same fin-actuation pattern. We elaborate on this below.

Simulations are first conducted using the original dynamic model with different sets of fin-beat parameters  $(\gamma_0, \gamma_A, T_P, \zeta)$ , where we use the identified body parameters (Tab. 1). Only the right fin is actuated, since the scaling functions are considered left-right symmetric. In particular, 560 simulations are conducted with the combination of the following fin-beat patterns: 7 different amplitudes  $(\gamma_{AR}): 10^{\circ}, 15^{\circ}, 20^{\circ}, 22^{\circ}, 25^{\circ}, 28^{\circ}, 30^{\circ}; 5$  different biases  $(\gamma_{0R}): 50^{\circ}, 60^{\circ}, 70^{\circ}, 80^{\circ}, 90^{\circ}; 4$  different periods  $(T_{pR}): 0.5, 0.66, 1, 2$  s; and 4 different power/recovery stroke ratios  $(\zeta): 2, 3, 4, 5$ .

For each simulation, we extract the turning radius R, turning period  $T_b$  (time taken to complete one turn) and angle of attack  $\alpha$  of the robot at the steady state, and then use the following relationships to determine the corresponding steady-state body-fixed linear  $(v_{c_x}, v_{c_y})$  and angular  $(\omega_z)$  velocities for the original dynamics:

$$T_b = \frac{2\pi}{\omega_z}, \quad R = \frac{\sqrt{v_{c_x}^2 + v_{c_y}^2}}{\omega_z}, \quad \alpha = \arctan\frac{v_{c_y}}{v_{c_x}}$$
 (29)

These velocities  $(v_{c_x}, v_{c_y}, \omega_z)$  are then considered as desired values to be tracked by the averaged model:  $\bar{v}_{xr} = v_{c_x}, \bar{v}_{yr} = v_{c_y}, \bar{\omega}_r = \omega_z$ . We further let  $u_1 = K_{f_xR}, u_2 = K_{f_yR}, u_3 = K_{m_R}$  such that (25) can be rewritten as

$$\dot{\bar{v}}_{c_x} = f_1 + u_1 \bar{f}_{h_x R} \tag{30}$$

$$\dot{\bar{v}}_{c_u} = f_2 + u_2 \bar{f}_{h_u R} \tag{31}$$

$$\dot{\bar{\omega}}_z = f_3 + u_3 \bar{\tau}_{h_R} \tag{32}$$

We construct the velocity tracking error as

$$e_{\eta} = \begin{bmatrix} \bar{v}_{c_x} - \bar{v}_{xr} \\ \bar{v}_{c_y} - \bar{v}_{yr} \\ \bar{\omega}_z - \bar{\omega}_r \end{bmatrix}$$
(33)

The objective is to determine  $u_1, u_2, u_3$  such that the tracking error states of system (33) are driven to zero. To do so, we define an objective function with the following stage cost  $F(\cdot)$  and terminal penalty  $E(\cdot)$ 

$$F(e_n, u) = e_n(\tau)^T Q e_n(\tau)$$
(34)

$$E(\boldsymbol{e}_{\boldsymbol{n}}(t+T)) = (\boldsymbol{e}_{\boldsymbol{n}}(t+T))^{T} Q_{T}(\boldsymbol{e}_{\boldsymbol{n}}(t+T))$$
(35)

where T is the prediction horizon,  $u(\tau) = [u_1 \ u_2 \ u_3]^T$ , and Q and  $Q_T$  are positive-definite weighting matrices that penalize deviations from the desired values. By solving the nonlinear model predictive control (NMPC) problem (for example, using ACADO Model Predictive Control Toolkit (Houska et al., 2011)), we obtain the optimal inputs  $u_1, u_2, u_3$  and thus the values for  $K_{f_xR}, K_{f_yR}, K_{m_R}$  for a given fin-beat parameter combination. Specifically, the following NMPC parameters are used in solving for the scaling values:

Length of optimization horizon : T=10 sSampling interval :  $t_s=1 \text{ s}$ Weighting matrix :  $Q=2000 I_3$ 

Terminal Penalty Weighting matrix:  $Q_T = 80 I_3$ 

where  $I_3$  is a 3 by 3 identity matrix. Fig. 3 shows the resultant 3D surfaces of optimal coefficients obtained for different fin amplitudes and fin biases when the fin actuation period and power/recover stroke ratio are fixed at some particular values. Results for other period and ratio combinations are similar and thus omitted in the interest of brevity.

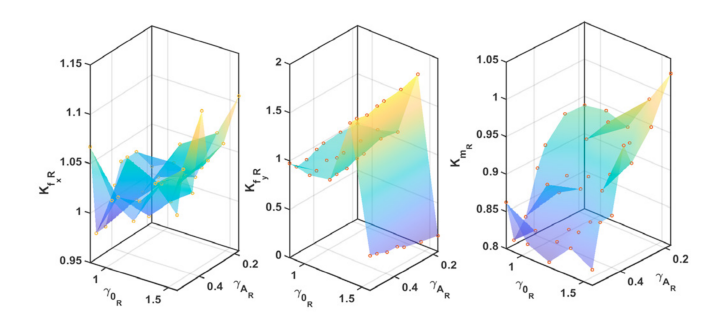


Fig. 3. Obtained scaling values  $K_{f_xR}$ ,  $K_{f_yR}$ ,  $K_{mR}$  versus the amplitude  $\gamma_{A_R}$  and bias  $\gamma_{0_R}$ , for fixed actuation period  $T_{p_R} = 1$  s and ratio  $\zeta = 2$ .

To obtain closed-form expressions for the relationships between each scaling coefficient and the fin-beat parameters, we implement a multivariate nonlinear regression scheme using the MATLAB command fitnlm, where we seek the lowest-degree polynomials that provide adequate match with the computed scaling coefficients, and obtain the following:

$$K_{f_xR} = 0.9801 - 0.0653\gamma_{A_R} + 0.0828\gamma_{0_R} \tag{36}$$

$$-0.0007\zeta_R - 0.0069T_{pR} \tag{37}$$

$$K_{f_yR} = -529.2 + 0.6\gamma_{A_R} + 1893.4\gamma_{0_R} - 3.8\gamma_{A_R}^2 - 2500.6\gamma_{0_R}^2 - 0.0000276\zeta_R^2 - 0.0001324T_{pR}^2 + 9.1\gamma_{A_R}^3 + 1446.6\gamma_{0_R}^3 - 8.2\gamma_{A_R}^4 - 309.1\gamma_{0_R}^4$$
(38)

$$K_{m_R} = 0.9869 - 0.4004\gamma_{A_R} + 0.0661\gamma_{0_R} - 0.0007\zeta_R - 0.0059T_{n_R}$$
(39)

## 4.4 Validation of the Averaged Model

We first compare the turning radius and period predictions between the averaged and the dynamic model for the turning case. Tab. 4 lists the errors between the predictions obtained from the averaged model and those obtained from the dynamic model for different sets of fin parameters. Furthermore, Fig. 5 depicts circular trajectories obtained from experiments and simulation using the dynamic and averaged models. From the figure, we can see how the trajectory behavior and steady-state radius of the dynamic and averaged model predictions match that of experiments, which suggest that the average model is able to capture well the behavior of the original dynamics and the dynamics of the robot under the new actuation patterns.

To further validate the average model, we conduct simulations and experiments considering the forward swimming motion. The forward swimming case was not used in obtaining the scaling functions, and thus provides independent validation for the proposed average model. Fig. 4 compares the simulated steady-state forward swimming speeds predicted with the original dynamic and the average models, and those obtained from the experiments. Note that the steady state is considered to be reached after the first 15 s of the robot swimming. In the experiments, for the given  $\zeta=4$ , to prevent exceeding the speed limit of the servo motors, a maximum actuation frequency 1.75 Hz is used. We have extended the simulation results to

Table 4. AVERAGED MODEL VALIDATION RESULTS: RELATIVE MODEL PREDICTION ERROR BETWEEN THE ORIGINAL AND AVERAGED MODELS FOR TURNING RADIUS AND TURNING PERIOD.

$(\gamma_{0L}, \gamma_{AL}, T_{pL}, \zeta_L)$	Turning Radius Error(%)	Turning Period Error(%)
(90°, 22°, 1 s, 4 )	3.51	0.21
(90°, 22°, 1 s, 3)	3.58	3.13
(90°, 20°, 1 s, 4 )	3.45	1.34
(90°, 20°, 1 s, 3)	3.77	5.58
(80°, 22°, 1 s, 4)	2.93	1.84
(80°, 22°, 1 s, 3)	3.31	2.56
$(80^{\circ}, 20^{\circ}, 1 \text{ s}, 4)$	2.86	0.73
$(80^{\circ}, 20^{\circ}, 1 \text{ s}, 3)$	3.78	2.17
$(60^{\circ}, 22^{\circ}, 1 \text{ s}, 4)$	2.14	4.06
$(60^{\circ}, 22^{\circ}, 1 \text{ s}, 3)$	2.29	2.00
$(60^{\circ}, 20^{\circ}, 1 \text{ s}, 4)$	1.97	0.19
$(60^{\circ}, 20^{\circ}, 1 \text{ s}, 3)$	2.28	4.60

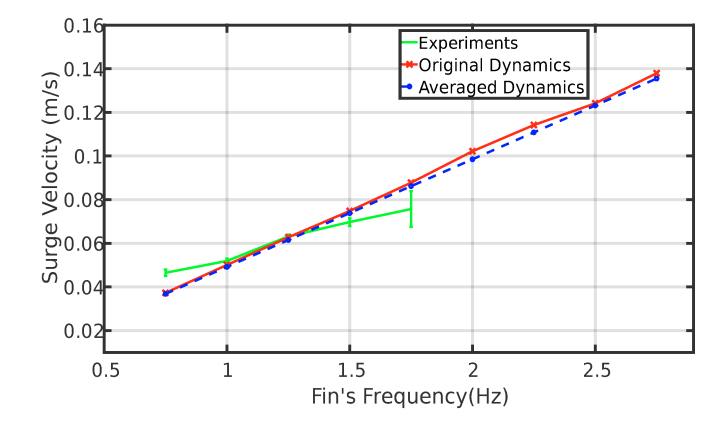


Fig. 4. Comparison between experimental results and the predictions of the steady-state forward swimming speed based on the average model and the original dynamic model. In this study the left and right fins undergo symmetric actuation with the following parameters fixed:  $\gamma_A = 15^{\circ}$ ,  $\gamma_0 = 95^{\circ}$  and  $\zeta = 4$ .

fin-beat frequency up to 2.75 Hz in order to capture the performance trend of the robotic fish.

#### 5. CONCLUSION

In this work, we presented a nonlinear dynamic average model for a pectoral fin-actuated robotic fish. In particular, we proposed a scaling averaging scheme, where the pectoral fin-generated hydrodynamic forces and moment are first scaled using functions of the fin-beat parameters, and classical averaging is then conducted over the resulting dynamics. Furthermore, we proposed a novel estimation scheme employing a nonlinear model predictive controller and a multivariate nonlinear regression scheme to determine the scaling functions. To evaluate the averaged model, simulation comparing the predictions from the original and average models were presented. Furthermore, both models were validated with experimental results.

For future work, the proposed averaging model will be utilized in a trajectory tracking control scheme to demonstrate its utility in feedback control of pectoral finactuated robotic fish. We will further explore the modeling and control of a robotic fish actuated by both pectoral and caudal fins, especially the optimal control policies to balance objectives in accuracy and energy-efficiency under different task requirements.

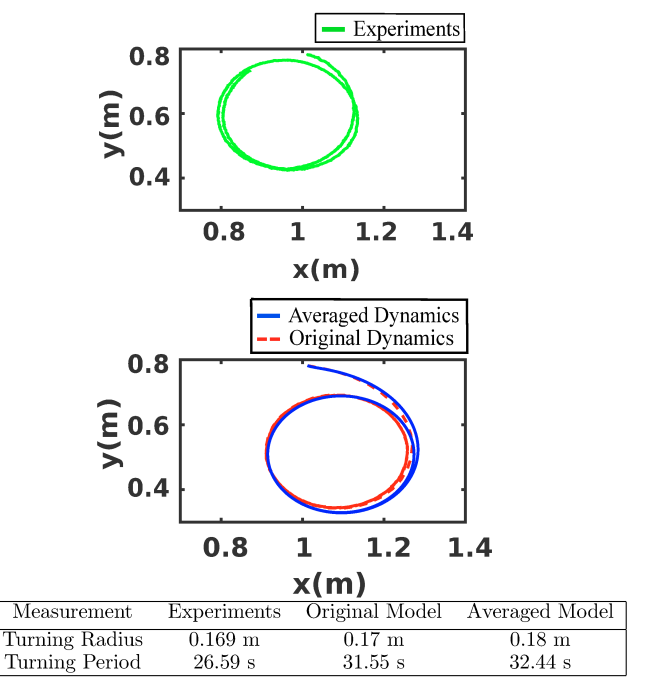


Fig. 5. Circular trajectories captured in experiments and predicted by the original and average dynamic models. In this case the right fin remains still and the left fin undergoes actuation with the following parameters fixed:  $\gamma_{AL} = 22^{\circ}$ ,  $\gamma_{0L} = 85^{\circ}$ ,  $T_{PL} = 1$  and  $\zeta = 4$ .

#### REFERENCES

Allgöwer, F., Findeisen, R., and Nagy, Z.K. (2004). Non-linear model predictive control: From theory to application. *J. Chin. Inst. Chem. Engrs*, 35(3), 299–315.

Aureli, M., Kopman, V., and Porfiri, M. (2009). Free-locomotion of underwater vehicles actuated by ionic polymer metal composites. *IEEE/ASME Transactions on Mechatronics*, 15(4), 603–614.

Behbahani, S.B. (2016). Role of Flexibility in Robotic Fish. Ph.D. thesis, Michigan State University.

Behbahani, S.B. and Tan, X. (2016). Design and modeling of flexible passive rowing joint for robotic fish pectoral fins. *IEEE Transactions on Robotics*, 32(5), 1119–1132.

Bi, S., Ma, H., Cai, Y., Niu, C., and Wang, Y. (2014). Dynamic modeling of a flexible oscillating pectoral fin for robotic fish. *Industrial Robot: An International Journal*, 41(5), 421–428.

Bullo, F. and Lewis, A.D. (2019). Geometric Control of Mechanical Systems: Modeling, Analysis, and Design for Simple Mechanical Control systems, volume 49. Springer.

Castaño, M.L. and Tan, X. (2019). Model predictive control-based path-following for tail-actuated robotic fish. *Journal of Dynamic Systems, Measurement, and Control*, 141(7).

Deng, X. and Avadhanula, S. (2005). Biomimetic micro underwater vehicle with oscillating fin propulsion: System design and force measurement. In *Proceedings of the 2005 IEEE International Conference on Robotics and Automation*, 3312–3317. IEEE.

Dong, R. (1978). Effective mass and damping of submerged structures. Technical report, California Univ., Livermore (USA). Lawrence Livermore Lab.

- Drucker, E.G., Walker, J.A., and Westneat, M.W. (2005). Mechanics of pectoral fin swimming in fishes. Fish Physiology, 23, 369–423.
- Duraisamy, P., Sidharthan, R.K., and Santhanakrishnan, M.N. (2019). Design, modeling, and control of biomimetic fish robot: A review. *Journal of Bionic Engineering*, 16(6), 967–993.
- Fossen, T.I. (1994). Guidance and Control of Ocean Vehicles. John Wiley & Sons Inc.
- Houska, B., Ferreau, H., and Diehl, M. (2011). ACADO
   Toolkit An Open Source Framework for Automatic
   Control and Dynamic Optimization. Optimal Control
   Applications and Methods, 32(3), 298–312.
- Kato, N. (1998). Locomotion by mechanical pectoral fins. Journal of Marine Science and Technology, 3(3), 113– 121.
- Kato, N. and Furushima, M. (1996). Pectoral fin model for maneuver of underwater vehicles. In *Proceedings of Symposium on Autonomous Underwater Vehicle Tech*nology, 49–56. IEEE.
- Kato, N. and Inaba, T. (1998). Guidance and control of fish robot with apparatus of pectoral fin motion. In Proceedings. 1998 IEEE International Conference on Robotics and Automation (Cat. No. 98CH36146), volume 1, 446–451. IEEE.
- Kodati, P., Hinkle, J., Winn, A., and Deng, X. (2008). Microautonomous robotic ostraciiform (MARCO): Hydrodynamics, design, and fabrication. *IEEE Transactions on Robotics*, 24(1), 105–117.
- Lachat, D., Crespi, A., and Ijspeert, A.J. (2006). Boxybot: a swimming and crawling fish robot controlled by a central pattern generator. In The First IEEE/RAS-EMBS International Conference on Biomedical Robotics and Biomechatronics, 2006. BioRob 2006., 643–648. IEEE.
- Lauder, G.V., Madden, P.G., Mittal, R., Dong, H., and Bozkurttas, M. (2006). Locomotion with flexible propulsors: I. Experimental analysis of pectoral fin swimming in sunfish. *Bioinspiration & Biomimetics*, 1(4), S25.
- Liu, X., Iwasaki, T., and Fish, F. (2013). Dynamic modeling and gait analysis of batoid swimming. In 2013 American Control Conference, 566–571. IEEE.
- Low, K. and Willy, A. (2006). Biomimetic motion planning of an undulating robotic fish fin. *Journal of Vibration* and Control, 12(12), 1337–1359.
- Marras, S. and Porfiri, M. (2012). Fish and robots swimming together: attraction towards the robot demands biomimetic locomotion. *Journal of The Royal Society Interface*, 9(73), 1856–1868.
- Mittal, R., Dong, H., Bozkurttas, M., Lauder, G., and Madden, P. (2006). Locomotion with flexible propulsors: II. computational modeling of pectoral fin swimming in sunfish. *Bioinspiration & Biomimetics*, 1(4), S35.
- Morgansen, K.A., Triplett, B.I., and Klein, D.J. (2007). Geometric methods for modeling and control of free-swimming fin-actuated underwater vehicles. *IEEE Transactions on Robotics*, 23(6), 1184–1199.
- Morgansen, K.A., Vela, P.A., and Burdick, J.W. (2002). Trajectory stabilization for a planar carangiform robot fish. In *Proceedings 2002 IEEE International Conference on Robotics and Automation (Cat. No. 02CH37292)*, volume 1, 756–762. IEEE.

- Palmisano, J., Ramamurti, R., Lu, K.J., Cohen, J., Sandberg, W., and Ratna, B. (2007). Design of a biomimetic controlled-curvature robotic pectoral fin. In *Proceedings* 2007 IEEE International Conference on Robotics and Automation, 966–973. IEEE.
- Sanders, J.A., Verhulst, F., and Murdock, J. (2007). Averaging Methods in Nonlinear Dynamical Systems, volume 59. Springer.
- Sfakiotakis, M., Lane, D.M., and Davies, J.B.C. (1999). Review of fish swimming modes for aquatic locomotion. *IEEE Journal of Oceanic Engineering*, 24(2), 237–252.
- Singh, N., Gupta, A., and Mukherjee, S. (2019). A dynamic model for underwater robotic fish with a servo actuated pectoral fin. SN Applied Sciences, 1(7), 659.
- Sitorus, P.E., Nazaruddin, Y.Y., Leksono, E., and Budiyono, A. (2009). Design and implementation of paired pectoral fins locomotion of labriform fish applied to a fish robot. *Journal of Bionic Engineering*, 6(1), 37–45.
- Tan, X. (2011). Autonomous robotic fish as mobile sensor platforms: Challenges and potential solutions. *Marine Technology Society Journal*, 45(4), 31–40.
- Valdivia y Alvarado, P. and Youcef-Toumi, K. (2005). Design of machines with compliant bodies for biomimetic locomotion in liquid environments. *Journal of Dynamic Systems, Measurement, and Control*, 128(1), 3–13. doi: 10.1115/1.2168476.
- Wang, J., McKinley, P.K., and Tan, X. (2015). Dynamic modeling of robotic fish with a base-actuated flexible tail. *Journal of Dynamic Systems, Measurement, and Control*, 137(1), 11004(1)–11004(11).
- Wang, J. and Tan, X. (2015). Averaging tail-actuated robotic fish dynamics through force and moment scaling. *IEEE Transactions on Robotics*, 31(4), 906–917. doi: 10.1109/TRO.2015.2433539.
- Ye, Z., Hou, P., and Chen, Z. (2017). 2D maneuverable robotic fish propelled by multiple ionic polymer-metal composite artificial fins. *International Journal of Intelligent Robotics and Applications*, 1(2), 195–208.
- Zhang, F., Ennasr, O., Litchman, E., and Tan, X. (2016). Autonomous sampling of water columns using gliding robotic fish: Algorithms and harmful-algae-sampling experiments. *IEEE Systems Journal*, 10(3), 1271–1281.
- Zhong, Y., Li, Z., and Du, R. (2018). Robot fish with two-DOF pectoral fins and a wire-driven caudal fin. Advanced Robotics, 32(1), 25–36.